Solvate Molecule Effects and Unusual ^{57}Fe Mössbauer Line Broadening in the Valence Detrapping of Mixed-Valence $[Fe_3O(O_2CCH_3)_6(3\text{-Et-py})_3]\cdot S$

Chi-Cheng Wu,[1] Ho Gyeom Jang,[1,2] Arnold L. Rheingold,[3] Philipp Gütlich,*[,4] and David N. Hendrickson*[,1]

Department of Chemistry-0358, University of California at San Diego, La Jolla, California 92093-0358, Department of Chemistry, University of Delaware, Newark, Delaware 19716, and Institut für Anorganische und Analytische Chemie, Johannes Gutenberg-Universität, D-55099 Mainz, Germany

Received November 9, 1995[⊗]

A new series of mixed-valence μ_3-oxo-bridged Fe_3O complexes with the composition $[Fe_3O(O_2CCH_3)_6(3\text{-Et-py})_3]\cdot S$, where 3-Et-py is 3-ethylpyridine and the solvate molecule S is either $0.5C_6H_5CH_3$ (**1**), $0.5C_6H_6$ (**2**), CH_3CN (**3**), or CH_3CCl_3 (**4**), is reported. The complex $[Fe_3O(O_2CCH_3)_6(3\text{-Et-py})_3]\cdot 0.5C_6H_5CH_3$ (**1**) crystallizes in the orthorhombic space group *Fdd*2 which at 298 K has a unit cell with $a = 22.726(8)$ Å, $b = 35.643(14)$ Å, $c = 20.816(6)$ Å, and $Z = 16$. Refinement with 5720 observed $[F > 5\sigma(F_o)]$ reflections gave $R = 0.0337$ and $R_w = 0.0390$. An analysis of the bond lengths in complex **1** shows that it is the most valence-trapped Fe_3O complex reported at room temperature. The complex $[Fe_3O(O_2CCH_3)_6(3\text{-Et-py})_3]\cdot CH_3CCl_3$ (**4**) crystallizes in the triclinic space group $P\bar{1}$ which at 238 K has a unit cell with $a = 12.764(2)$ Å, $b = 13.1472(2)$ Å, $c = 15.896(3)$ Å, $\alpha = 78.01(2)°$, $\beta = 89.38(2)°$, $\gamma = 61.38(1)°$, and $Z = 2$. Refinement with 6264 observed $[F > 5\sigma(F_o)]$ reflections gave $R = 0.0435$ and $R_w = 0.0583$. In this μ_3-oxo-bridged complex all three iron ions are inequivalent. Powder X-ray diffraction patterns taken at room temperature show that complexes **1** and **2** are isostructural and that complexes **3** and **4** are isostructural. Variable-temperature ^{57}Fe Mössbauer spectra were collected for all four complexes. The data for complexes **1** and **2** clearly indicate that these two complexes are totally valence trapped. On the other hand, Mössbauer spectra (43−293 K) for complexes **3** and **4** show that these two complexes become valence detrapped at temperatures near room temperature. Two doublets are seen at low temperature and they move together to become a single doublet at ∼293 K. Examination of the line width versus temperature for each of the two components of the two doublets points to a curiosity. The two components of the "Fe^{III}" doublet and the lower-velocity component of the "Fe^{II}" doublet do not exhibit any line broadening, whereas the higher velocity "Fe^{II}" component shows a surge in line width in the ∼70−150 K range. Possible explanations for these unusual line width responses are discussed.

Introduction

The study of intramolecular electron transfer events in mixed-valence complexes in the solid state can provide fundamental information about environmental effects on the rates of electron transfer. With detailed structural, spectroscopic, and thermodynamic data it has been shown possible to characterize some important environmental factors affecting the rate of intramolecular electron transfer.[5] Recent studies on a series of mixed-valence trinuclear iron acetate[6] and dinuclear biferrocenium complexes[7] clearly indicate that the detailed nature of the solid state environment about a mixed-valence complex can be the most important factor in determining the rate of intramolecular electron transfer.

The pronounced impact that lattice environments have on the rate of electron transfer has been established in the studies of several mixed-valence $[Fe^{II}Fe^{III}_2O(O_2CCH_3)_6(L)_3]\cdot S$ complexes, where L is a ligand such as H_2O or (substituted) pyridine and S is a solvate molecule. For the "stacked" structure (*R*32 space group symmetry) found in these Fe_3O complexes both the positioning and the size of solvate molecule affect the valence detrapping of Fe_3O complexes.[6k,l] In the stacks of these Fe_3O complexes, each solvate molecule (*e.g.*, $CHCl_3$) is sandwiched between two Fe_3O complexes where only van der Waals interactions occur. When the asymmetric environment about an Fe_3O complex makes the zero-point energy differences among the ($Fe^{II}_aFe^{III}_bFe^{III}_c$), ($Fe^{III}_aFe^{II}_bFe^{III}_c$), and ($Fe^{III}_aFe^{III}_bFe^{II}_c$) vibronic states appreciable, the rate of tunneling between the vibronic sates is decreased.[5a]

There are two types of intermolecular interactions present in these stacked Fe_3O complexes.[5b] Clearly the strongest intermolecular interaction occurs between Fe_3O complexes in neighboring stacks. There is an overlapping of pyridine ligands. This py···py interstack interaction is affected by the solvate molecule S. Experimental data[5d,6c,d,i,j] and theoretical models[6f,8] indicate that valence-detrapping events occur in phase transitions. The second type of intermolecular interaction occurs between Fe_3O complexes in one stack. Since the in-stack interactions between Fe_3O complexes are propagated by the solvate molecules, the exact nature of the solvate molecule can subtly affect valence detrapping. Solid-state ^{2}H NMR studies have shown[6c,e,g,h,k,l] that the orientation of the solvate molecule

[⊗] Abstract published in *Advance ACS Abstracts,* June 1, 1996.

(1) University of California at San Diego.
(2) Korea University.
(3) University of Delaware.
(4) Johannes-Gutenberg Universität.
(5) (a) Hendrickson, D. N.; Oh, S. M.; Dong, T.-Y.; Kambara, T.; Cohn, M. J.; Moore, M. F. *Comments Inorg. Chem.* **1985**, *4*, 329. (b) Hendrickson, D. N. Electron Transfer in Mixed-Valence Complexes in the Solid State. In *Mixed-Valency Systems: Applications in Chemistry, Physics and Biology*; NATO ASI Series C: Mathematical and Physical Sciences 343; Prassides, K., Ed.; Kluwer Academic Publishers: Dordrecht, The Netherlands, 1991; p 67−90. (c) Cannon, R. D.; Jayasooria, U. A.; White, R. P. Inelastic Neutron Scattering Studies of Mixed-Valency Compounds. In *Mixed-Valency Systems: Applications in Chemistry, Physics and Biology*; NATO ASI Series C: Mathematical and Physical Sciences 343; Prassides, K., Ed.; Kluwer Academic Publishers: Dordrecht, The Netherlands, 1991; p 283−298. (d) Sorai, M.; Hendrickson, D. N. *Pure Appl. Chem.* **1991**, *63*, 1503.

S0020-1669(95)01450-9 CCC: $12.00

and whether it is static or dynamic affect the valence detrapping. In a series of isostructural (*R*32 symmetry) $[Fe_3O(O_2CCH_3)_6(4\text{-Me-py})_3]\cdot S$ complexes[6k] where the solvate molecules are C_6H_6, $CHCl_3$, CH_3CCl_3 and CH_3CHCl_2, the Fe_3O complex with a bulky solvate molecule (CH_3CCl_3) or lower symmetry solvate molecule (CH_3CHCl_2) shows a higher valence-detrapping temperature than that of a complex with a smaller and more symmetric solvate molecule ($CHCl_3$). *It must be emphasized that these Fe_3O complexes never become electronically delocalized*. At higher temperatures they may become valence detrapped. There are still barriers for interconversion, but the thermal energy becomes large enough to exhibit an appreciable rate of interconversion. This is conclusively indicated by IR spectroscopy.[6q−t]

In the second structural type of Fe_3O complexes, the solvate molecule is located in a cavity formed from three Fe_3O molecules which are arranged two-dimensionally in a layer. This "layer" structure has been found[6h] in $[Fe_3O(O_2CCH_3)_6(3\text{-Me-py})_3]\cdot S$ complexes, where S is either 3-Me-py (3-methylpyridine), benzene, or toluene. For these complexes there are no strong intermolecular interactions in evidence, certainly no (3-Me-py)···(3-Me-py) contacts. In spite of the weak intermolecular interactions and the asymmetric environment provided by the solvate molecules, the positioning of the solvate molecules can also lead to valence detrapping in these layer Fe_3O complexes. The weak interactions of a solvate molecule with a neighboring Fe_3O complex are influential in affecting electron transfer in these complexes. In fact, for all systems of Fe_3O complexes studied,[5,6] there is always an onset of solvate molecule motion associated with a phase transition accompanying the valence-detrapping event (electron transfer). There is not as much work done on layer Fe_3O complexes as on those that assume the stacked structure.

In all mixed-valence Fe_3O complexes and biferrocenium salts studied, there is no line broadening observed in the variable-temperature Mössbauer spectra in the temperature region where the complexes become valence detrapped. It has been suggested that the onset of lattice dynamics controls the valence detrapping by modulating the relative vibronic levels.[5b,d] If both the rate of electron transfer and lattice dynamics are faster than the Mössbauer time scale, the low-temperature Fe^{II} and Fe^{III} doublets would just move together to become a single average doublet and no line broadening would be seen. It would be interesting to slow down either of these processes, electron transfer or lattice dynamics, to a rate comparable with the ^{57}Fe Mössbauer spectroscopic time scale such that more information can be revealed.

In this paper results are presented for a series of complexes $[Fe_3O(O_2CCH_3)_6(4\text{-Et-py})_3]\cdot S$ where S is $0.5C_6H_5CH_3$, $0.5C_6H_6$, CH_3CN, or CH_3CCl_3. It was of interest to obtain more data regarding the effects of solvate molecules on valence detrapping in layer Fe_3O complexes and to examine closely the line widths of ^{57}Fe Mössbauer signals for such complexes undergoing a valence-detrapping conversion. Another goal in this research was to characterize a mixed-valence Fe_3O complex that is totally valence trapped throughout the 4−350 K region.

Experimental Section

Compound Preparation. 3-Ethylpyridine was dried by refluxing over BaO and then fractionally distilled under an argon atmosphere, benzene and toluene were dried by refluxing with Na/benzophenone under a nitrogen atmosphere, and acetonitrile was dried over P_2O_5 and distilled under an argon atmosphere. 1,1,1-Trichloroethane was used directly from a Sure/Seal bottle purchased from Aldrich. Elemental analyses were performed by Oneida Research Service, Inc. Purified solvents and dried compounds were always stored and manipulated under an argon atmosphere.

$[Fe_3O(O_2CCH_3)_6(H_2O)_3]$. This mixed-valence compound was prepared according to a modification of a previously reported method.[9] A solution of 30 g (0.15 mol) of $FeCl_2\cdot 4H_2O$ in 150 mL of water was placed in a 500 mL three-neck flask. To this solution was added a suspension of 30 g (0.366 mol) of CH_3COONa in 90 mL (1.57 mol) of glacial acetic acid. The reaction mixture was heated at 70−75 °C under reflux for 2 h, with bubbling of a constant stream of air. The mixture was cooled to room temperature, and the dark-brown precipitate was filtered off, washed with ethanol and ethyl ether, and dried under vacuum for 3 days. The yield was 15.6 g (52.7%). Anal. Calcd for $C_{12}H_{24}O_{16}Fe_3$: C, 24.35; H, 4.09; Fe, 28.31. Found: C, 24.09; H, 4.18; Fe, 27.89.

$[Fe_3O(O_2CCH_3)_6(3\text{-Et-py})_3]\cdot 3\text{-Et-py}$. The sample of this compound was prepared by dissolving 5.0 g (8.5 mmol) of $[Fe_3O(O_2CCH_3)_6(H_2O)_3]$ in 30 mL of 3-ethylpyridine and stirring for 1 h at 60−65 °C under an argon atmosphere. The solution was then cooled to room temperature and slowly evaporated for 3 days. The black crystalline product was filtered off and dried under vacuum [yield was 5.73 g (69.8%)]. Anal. Calcd for $C_{40}H_{54}N_4Fe_3O_{13}$: C, 49.72; H, 5.59; N, 5.80; Fe, 17.34. Found: C, 49.71; H, 5.72; N, 5.72; Fe, 17.39.

$[Fe_3O(O_2CCH_3)_6(3\text{-Et-py})_3]\cdot 0.5(\text{toluene})$ (1), $[Fe_3O(O_2CCH_3)_6(3\text{-Et-py})_3]\cdot 0.5(\text{benzene})$ (2), $[Fe_3O(O_2CCH_3)_6(3\text{-Et-py})_3]\cdot CH_3CN$ (3), and $[Fe_3O(O_2CCH_3)_6(3\text{-Et-py})_3]\cdot CH_3CCl_3$ (4). These compounds were prepared by recrystallizing $[Fe_3O(O_2CCH_3)_6(3\text{-Et-py})_3]\cdot 3\text{-Et-py}$

(6) (a) Oh, S. M.; Hendrickson, D. N.; Hassett, K. L.; Davis, R. E. *J. Am. Chem. Soc.* **1984**, *106*, 7984. (b) Oh, S. M.; Hendrickson, D. N.; Hassett, K. L.; Davis, R. E. *J. Am. Chem. Soc.* **1985**, *107*, 8009. (c) Oh, S. M.; Kambara, T.; Hendrickson, D. N.; Sorai, M.; Kaji, K.; Woehler, S. E.; Wittebort, R. J. *J. Am. Chem. Soc.* **1985**, *107*, 5540. (d) Sorai, M.; Kaji, K.; Hendrickson, D. N.; Oh, S. M. *J. Am. Chem. Soc.* **1986**, *108*, 702. (e) Woehler, S. E.; Wittebort, R. J.; Oh, S. M.; Hendrickson, D. N.; Inniss, D.; Strouse, C. E. *J. Am. Chem. Soc.* **1986**, *108*, 2938. (f) Kambara, T.; Hendrickson, D. N.; Sorai, M.; Oh, S. M. *J. Chem. Phys.* **1986**, *85*, 2895. (g) Woehler, S. E.; Wittebort, R. J.; Oh, S. M.; Kambara, T.; Hendrickson, D. N.; Inniss, D.; Strouse, C. E. *J. Am. Chem. Soc.* **1987**, *109*, 1063. (h) Oh, S. M.; Wilson, S. R.; Hendrickson, D. N.; Woehler, S. E.; Wittebort, R. J.; Inniss, D.; Strouse, C. E. *J. Am. Chem. Soc.* **1987**, *109*, 1073. (i) Sorai, M.; Shiomi, Y.; Hendrickson, D. N.; Oh, S. M.; Kambara, T. *Inorg. Chem.* **1987**, *26*, 223. (j) Kaneko, Y.; Nakano, M.; Sorai, M.; Jang, H. G.; Hendrickson, D. N. *Inorg. Chem.* **1989**, *28*, 1067. (k) Jang, H. G.; Geib, S. J.; Kaneko, Y.; Nakano, M.; Sorai, M.; Rheingold, A. L.; Montez, B.; Hendrickson, D. N. *J. Am. Chem. Soc.* **1989**, *111*, 173. (l) Jang, H. G.; Wittebort, R. J.; Sorai, M.; Kaneko, Y.; Nakano, M.; Hendrickson, D. N. *Inorg. Chem.* **1992**, *31*, 2265. (m) Cannon, R. D.; Jayasooria, U. A.; Arap Koske, S. K.; White, R. P.; Williams, J. H. *J. Am. Chem. Soc.* **1991**, *113*, 4158. (n) Nakamoto, T.; Katada, M.; Kawata, S.; Kitagawa, S.; Kikuchi, K.; Ikemoto, I.; Endo, K.; Sano, H. *Chem. Lett.* **1993**, 1463. (o) Nakamoto, T.; Katada, M.; Kawata, S.; Kitagawa, S.; Sano, H.; Konno, M. *Hyperfine Interact.* **1994**, *93*, 1567. (p) Cannon, R. D.; White, R. P. *Prog. Inorg. Chem.* **1988**, *36*, 195. (q) Cannon R. D.; Montri, L.; Brown, D. B.; Marshall, K. M.; Elliott, C. M. *J. Am. Chem. Soc.* **1984**, *106*, 2591. (r) Meesuk, L.; Jayasooriya, U. A.; Cannon, R. D. *J. Am. Chem. Soc.* **1987**, *109*, 2009. (s) Wu, R.; Arap Koske, S. K.; White, R. P.; Anson, C. E.; Jayasooriya, U. A.; Cannon, R. D. *J. Chem. Soc., Chem. Commun.* **1994**, 1657. (t) White, R. P.; Wilson, L. M.; Williamson, D. J.; Moore, G. R.; Jayasooriya, U. A.; Cannon, R. D. *J. Chem. Soc., Chem. Commun.* **1994**, 1657.

(7) (a) Dong, T.-Y.; Cohn, M. J.; Hendrickson, D. N.; Pierpont, C. G. *J. Am. Chem. Soc.* **1985**, *107*, 4777. (b) Cohn, M. J.; Dong, T.-Y.; Hendrickson, D. N.; Geib, S. J.; Rheingold, A. L. *J. Chem. Soc., Chem. Commun.* **1985**, 1095. (c) Dong, T.-Y.; Hendrickson, D. N.; Iwai, K.; Cohn, M. J.; Rheingold, A. L.; Sano, H.; Motoyama, I.; Nakashima, S. *J. Am. Chem. Soc.* **1985**, *107*, 7996. (d) Dong, T.-Y.; Hendrickson, D. N.; Pierpont, C. G.; Moore, M. F. *J. Am. Chem. Soc.* **1986**, *108*, 963. (e) Moore, M. F.; Wilson, S. R.; Cohn, M. J.; Dong, T.-Y.; Mueller-Westerhoff, U. T.; Hendrickson, D. N. *Inorg. Chem.* **1985**, *24*, 4559. (f) Dong, T.-Y.; Kambara, T.; Hendrickson, D. N. *J. Am. Chem. Soc.* **1986**, *108*, 4423. (g) Dong, T.-Y.; Kambara, T.; Hendrickson, D. N. *J. Am. Chem. Soc.* **1986**, *108*, 5857. (h) Sorai, M.; Nishimori, A.; Hendrickson, D. N.; Dong, T.-Y.; Cohn, M. J. *J. Am. Chem. Soc.* **1987**, *109*, 4266. (i) Kambara, T.; Hendrickson, D. N.; Dong, T.-Y.; Cohn, M. J. *J. Chem. Phys.* **1987**, *86*, 2362.

(8) Stratt, R. M.; Adachi, S. H. *J. Chem. Phys.* **1987**, *86*, 7156.

(9) Johnson, M. K.; Cannon, R. D.; Powell, D. B. *Spectrochim. Acta* **1982**, *38A*, 307.

Table 1. Crystallographic Data for $[Fe_3O(O_2CCH_3)_6(3\text{-Et-py})_3]\cdot 0.5(\text{toluene})$ (**1**) and $[Fe_3O(O_2CCH_3)_6(3\text{-Et-py})_3]\cdot CH_3CCl_3$ (**4**)

	complex **1**	complex **4**
empirical formula	$C_{36.5}H_{49}Fe_3N_3O_{13}$	$C_{35}H_{51}Cl_3Fe_3N_3O_{13}$
fw	904.74	995.7
crystal system	orthorhombic	triclinic
space group	*Fdd*2	$P\bar{1}$
a, Å	22.726(8)	12.764(2)
b, Å	35.643(14)	13.147(2)
c, Å	20.816(6)	15.896(3)
α, deg	90.0	78.01(2)
β, deg	90.0	89.38(2)
γ, deg	90.0	61.38(1)
V, Å^3	16862(9)	2278.2(8)
Z	16	2
μ, cm^{-1}	11.1	11.77
d(calcd), g/cm^3	1.43	1.449
temp, K	298	238
radiation; λ, Å	Mo Kα; 0.7107	Mo Kα; 0.7107
no. of total unique data	7078	8682
no. of unique data for $F_o > 5\sigma(F_o)$	5720	6264
R	0.0337	0.0435
R_w	0.0390	0.0583
goodness of fit	0.971	1.30

in toluene, benzene, CH_3CN, and CH_3CCl_3, respectively. Anal. Calcd for $[Fe_3O(O_2CCH_3)_6(3\text{-Et-py})_3]\cdot 0.5(\text{toluene})$: C, 48.41; H, 5.42; N, 4.64; Fe, 18.52. Found: C, 49.71; H, 5.72; N, 5.00; Fe, 18.73. Anal. Calcd for $[Fe_3O(O_2CCH_3)_6(3\text{-Et-py})_3]\cdot 0.5(\text{benzene})$: C, 48.13; H, 5.53; N, 4.68; Fe, 18.67. Found: C, 47.79; H, 5.03; N, 4.83; Fe, 18.85. Calcd for $[Fe_3O(O_2CCH_3)_6(3\text{-Et-py})_3]\cdot CH_3CN$: C, 46.70; H, 5.34; N, 6.23; Fe, 18.61. Found: C, 46.81; H, 5.28; N, 6.26; Fe, 18.71. Calcd for $[Fe_3O(O_2CCH_3)_6(3\text{-Et-py})_3]\cdot CH_3CCl_3$: C, 42.34; H, 4.84; N, 4.23; Fe, 16.88; Cl, 10.64. Found: C, 41.99; H, 4.99; N, 4.30; Fe, 16.56, Cl, 11.01.

Physical Measurements: Variable-Temperature ^{57}Fe Mössbauer Spectroscopy. Variable-temperature Mössbauer spectra were obtained in vertical transmission geometry by using a constant-acceleration spectrometer which has been described before.[10] The sample temperature was controlled by a Lake Shore Cryotronics Model DRC80C temperature controller in conjunction with a silicon diode mounted on the copper sample cell holder and is estimated to have an absolute accuracy of ±3 K. Computer fittings of Mössbauer data to Lorentzian line shapes were carried out with a modified version of a previously reported[11] computer program for complexes **1**−**3**. Mössbauer spectra for complex **4** were fitted to Lorentzian line shapes using the program MOSFUN (Mössbauer Spectra Fitting Program for Universal Theories).[12] The isomer shift values are reported relative to iron foil at 298 K but are not corrected for the temperature-dependent second-order Doppler shift.

Crystal Measurements, Data Collection, and X-ray Structure Refinements for $[Fe_3O(O_2CCH_3)_6(3\text{-Et-py})_3]\cdot 0.5(\text{toluene})$ (1) and $[Fe_3O(O_2CCH_3)_6(3\text{-Et-py})_3]\cdot CH_3CCl_3$ (4). Crystallographic data are collected in Table 1. For $[Fe_3O(O_2CCH_3)_6(3\text{-Et-py})_3]\cdot 0.5C_7H_8$ (**1**), systematic absences in the intensity data and diffraction symmetry determined this complex to belong to the orthorhombic space group *Fdd*2. Data were collected for a 0.31 × 0.31 × 0.35 mm crystal at 298 K on a Nicolet R3 automated diffractometer in the range $4 \le 2\theta \le 51°$. The unit cell parameters, listed in Table 1, were obtained by a least-squares fit to the automatically centered settings of 50 reflections, $22 \le 2\theta \le 26°$. Data were corrected for Lorentz, polarization, and anomalous dispersion effects. The structure of complex **1** was solved by an interpreted Patterson procedure which located the Fe atoms; the remaining non-hydrogen atoms were obtained from subsequent difference Fourier syntheses. Refinement of the structure included anisotropic temperature parameters for non-hydrogen atoms. Hydrogen atoms were incorporated as fixed idealized isotropic contributions [*d*(C−H) = 0.96 Å]. The final positional parameters for all refined atoms of complex **1** are listed in Table 2.

Table 2. Positional Parameters for $[Fe_3O(O_2CCH_3)_6(3\text{-Et-py})_3]\cdot 0.5(\text{toluene})$ (**1**) at 298 K

atom	*x*/*a*	*y*/*b*	*z*/*c*
Fe(1)	0.0002(1)	0.3032(1)	0.5000
Fe(2)	−0.0190(1)	0.3124(1)	0.3452(1)
Fe(3)	0.0145(1)	0.2285(1)	0.4056(1)
N(1)	−0.0005(2)	0.3309(1)	0.5972(2)
N(2)	−0.0428(2)	0.3494(1)	0.2616(2)
N(3)	0.0355(2)	0.1673(1)	0.3929(2)
O(1)	0.0455(2)	0.3514(1)	0.4756(2)
O(2)	0.0334(2)	0.3571(1)	0.3698(2)
O(3)	−0.0772(2)	0.3320(1)	0.4918(2)
O(4)	−0.0886(2)	0.3401(1)	0.3864(2)
O(5)	0.0476(2)	0.2938(1)	0.2873(2)
O(6)	0.0691(2)	0.2377(1)	0.3263(2)
O(7)	−0.0765(2)	0.2762(1)	0.3033(2)
O(8)	−0.0599(2)	0.2198(1)	0.3457(2)
O(9)	0.0903(2)	0.2314(1)	0.4655(2)
O(10)	0.0777(2)	0.2804(1)	0.5301(2)
O(11)	−0.0362(2)	0.2117(1)	0.4841(2)
O(12)	−0.0434(2)	0.2618(1)	0.5473(2)
O(13)	−0.0014(2)	0.2835(1)	0.4174(2)
C(1)	0.0529(3)	0.3678(2)	0.4231(4)
C(2)	0.0862(4)	0.4042(2)	0.4240(4)
C(3)	−0.1035(3)	0.3447(2)	0.4441(4)
C(4)	−0.1579(3)	0.3673(2)	0.4566(4)
C(5)	0.0779(3)	0.2643(2)	0.2906(3)
C(6)	0.1295(4)	0.2612(2)	0.2459(3)
C(7)	−0.0861(4)	0.2419(2)	0.3091(3)
C(8)	−0.1348(4)	0.2258(2)	0.2674(3)
C(9)	0.1069(3)	0.2529(2)	0.5088(4)
C(10)	0.1649(3)	0.2462(2)	0.5414(3)
C(11)	−0.0503(3)	0.2272(2)	0.5343(3)
C(12)	−0.0807(3)	0.2044(2)	0.5847(3)
C(21)	0.0070(3)	0.3122(2)	0.6515(3)
C(22)	0.0049(4)	0.3284(3)	0.7111(4)
C(23)	−0.0050(4)	0.3665(2)	0.7151(4)
C(24)	−0.0136(5)	0.3866(2)	0.6594(4)
C(25)	−0.0108(4)	0.3673(2)	0.6017(4)
C(26)	−0.0129(7)	0.4349(4)	0.6558(8)
C(27)	−0.0627(7)	0.4398(5)	0.6430(10)
C(31)	−0.0538(3)	0.3861(2)	0.2710(3)
C(32)	−0.0718(3)	0.4100(2)	0.2218(3)
C(33)	−0.0786(3)	0.3952(2)	0.1608(3)
C(34)	−0.0686(3)	0.3575(2)	0.1400(3)
C(35)	−0.0489(3)	0.3358(2)	0.2055(3)
C(36)	−0.0718(3)	0.3393(2)	0.0827(3)
C(37)	−0.1214(4)	0.3546(2)	0.0423(3)
C(41)	0.0841(3)	0.1561(2)	0.3635(3)
C(42)	0.1007(4)	0.1189(2)	0.3572(3)
C(43)	0.0642(3)	0.0922(2)	0.3851(4)
C(44)	0.0127(3)	0.1027(2)	0.4150(3)
C(45)	0.0004(3)	0.1413(2)	0.4178(3)
C(46)	−0.0301(4)	0.0739(2)	0.4492(4)
C(47)	−0.0422(4)	0.0817(2)	0.5174(4)
C(51)	0.5000	0.0000	0.1539(7)
C(52)	0.4529(5)	0.0143(2)	0.1875(5)
C(53)	0.4528(4)	0.0148(2)	0.2549(5)
C(54)	0.5000	0.0000	0.2892(6)
C(55)	0.5000	0.0000	0.3576(7)

For $[Fe_3O(O_2CCH_3)_6(3\text{-Et-py})_3](3\text{-Et-py})\cdot CH_3CCl_3$ (**4**), no evidence for symmetry higher than triclinic was found in the diffraction or photographic data or by cell reduction routines. Data were collected on a 0.30 × 0.30 × 0.35 mm crystal in the range $4 \le 2\theta \le 52°$. The centrosymmetric alternative, $P\bar{1}$, was chosen initially on the basis of its statistical preference and was later supported by chemically reasonable results from the refinement. Because ψ-scan data showed a <10% variation, no correction for absorption was performed. The structure of complex **4** was solved by direct methods. All non-hydrogen atoms were anisotropically refined, and all hydrogen atoms (except for those in the solvent molecule) were idealized. The 1,1,1-trichloroethane solvate molecule is disordered in two resolvable orientations in an

(10) Cohn, M. J.; Timken, M. D.; Hendrickson, D. N. *J. Am. Chem. Soc.* **1984**, *106*, 6683.
(11) Chrisman, B. L.; Tumolillo, T. A. *Comput. Phys. Commun.* **1971**, *2*, 322.
(12) Müller, E. W. *Mössbauer Eff. Ref. Data J.* **1981**, *4*, 89.

Table 3. Positional Parameters for $[Fe_3O(O_2CCH_3)_6(3\text{-Et-py})_3]\cdot CH_3CCl_3$ (**4**) at 238 K

atom	*x*/*a*	*y*/*b*	*z*/*c*
Fe(1)	0.66651(5)	0.37685(5)	0.2704(3)
Fe(2)	0.46211(5)	0.66177(5)	0.22140(3)
Fe(3)	0.38053(5)	0.45486(5)	0.25819(3)
N(1)	0.8542(3)	0.2260(3)	0.2920(2)
N(2)	0.4235(3)	0.8504(3)	0.1904(2)
N(3)	0.2323(3)	0.4091(3)	0.2679(2)
O(1)	0.5029(2)	0.4956(2)	0.2512(2)
O(121)	0.7228(2)	0.4480(2)	0.3518(2)
O(122)	0.5830(3)	0.6388(2)	0.3189(2)
O(123)	0.7274(3)	0.4528(2)	0.1690(2)
O(124)	0.5847(3)	0.6428(2)	0.1310(2)
O(131)	0.6464(2)	0.2752(3)	0.3801(2)
O(132)	0.4520(2)	0.3294(3)	0.3730(2)
O(133)	0.6449(2)	0.2834(3)	0.1899(2)
O(134)	0.4532(2)	0.3277(3)	0.1867(2)
O(231)	0.3296(2)	0.7153(2)	0.3068(2)
O(232)	0.2793(2)	0.5715(2)	0.3316(2)
O(233)	0.3368(2)	0.7102(2)	0.1190(2)
O(234)	0.2803(3)	0.5713(3)	0.1478(2)
C(121)	0.6745(3)	0.5527(3)	0.3612(2)
C(122)	0.7322(5)	0.5755(4)	0.4323(3)
C(123)	0.6810(3)	0.5565(3)	0.1220(2)
C(124)	0.7480(5)	0.5776(5)	0.0477(3)
C(131)	0.5563(3)	0.2753(3)	0.4106(2)
C(132)	0.5747(4)	0.2032(4)	0.5019(3)
C(133)	0.5554(3)	0.2811(3)	0.1612(2)
C(134)	0.5734(4)	0.2142(5)	0.0914(3)
C(231)	0.2742(3)	0.6650(3)	0.3439(2)
C(232)	0.1930(4)	0.7202(4)	0.4099(3)
C(233)	0.2789(3)	0.6614(3)	0.1017(2)
C(234)	0.1984(4)	0.7165(4)	0.0176(3)
C(11)	0.9134(3)	0.1957(3)	0.2230(3)
C(12)	1.0298(3)	0.1045(4)	0.2286(3)
C(13)	1.0870(4)	0.0401(4)	0.3101(3)
C(14)	1.0268(4)	0.0693(4)	0.3818(3)
C(15)	0.9119(4)	0.1623(4)	0.3702(3)
C(16)	1.0890(4)	0.0791(4)	0.1469(3)
C(17)	1.0848(6)	-0.0213(5)	0.1200(4)
C(21)	0.4154(3)	0.9044(3)	0.2544(3)
C(22)	0.3971(4)	1.0197(4)	0.2425(3)
C(23)	0.3860(4)	1.0810(4)	0.1585(3)
C(24)	0.3941(4)	1.0272(4)	0.0917(3)
C(25)	0.4128(4)	0.9117(4)	0.1100(3)
C(26)	0.3947(6)	1.0705(4)	0.3198(3)
C(27)	0.5167(7)	1.0322(6)	0.3587(4)
C(31)	0.1943(3)	0.3862(3)	0.3447(3)
C(32)	0.0999(4)	0.3629(4)	0.3564(3)
C(33)	0.0409(4)	0.3658(4)	0.2828(3)
C(34)	0.0812(5)	0.3863(5)	0.2034(3)
C(35)	0.1761(4)	0.4076(4)	0.1986(3)
C(36)	0.0607(5)	0.3305(5)	0.4462(3)
C(37)	0.1608(6)	0.2099(6)	0.4977(4)
Cl(1)	0.7382(3)	0.7827(3)	0.2202(2)
Cl(2)	0.8483(3)	0.8569(3)	0.0896(1)
Cl(3)	0.8310(2)	0.9326(2)	0.2450(2)
Cl(4)	0.9599(22)	0.6886(22)	0.2727(15)
C(1S)	0.8519(5)	0.8130(6)	0.2010(4)
C(2S)	0.9916(10)	0.7101(9)	0.2398(14)
C(2S′)	0.9778(30)	0.7095(29)	0.2222(22)

approximate 85/15 ratio in which two Cl atoms remain fixed and the third Cl and methyl group exchange positions. The final positional parameters for all refined atoms of complex **4** are listed in Table 3.

All computations used the SHELXTL (PC-version 4.2) library of crystallographic software (G. Sheldrick, Siemens, Madison, WI). Tables of detailed bond lengths and bond angles, anisotropic thermal parameters, and hydrogen atom coordinates for both complexes **1** and **4** are given in the Supporting Information.

Results and Discussion

Single-Crystal X-ray Structures of Complexes 1 and 4. The molecular and crystal structures of $[Fe_3O(O_2CCH_3)_6(3\text{-Et-py})_3]\cdot 0.5$toluene (**1**) and $[Fe_3O(O_2CCH_3)_6(3\text{-Et-py})_3]\cdot CH_3CCl_3$ (**4**) were determined. Previous work[6] has indicated that changing the solvate molecule can have a dramatic effect on the rate of intramolecular electron transfer in these mixed-valence iron acetates. It will be shown that complex **4** converts from valence trapped at low temperatures to valence detrapped at room temperature. On the other hand, complex **1** remains valence trapped throughout the 57−350 K range. It was desirable to determine the X-ray structure of complex **1** because ^{57}Fe Mössbauer data indicate that this complex is one of the most valence-trapped Fe_3O complexes known.

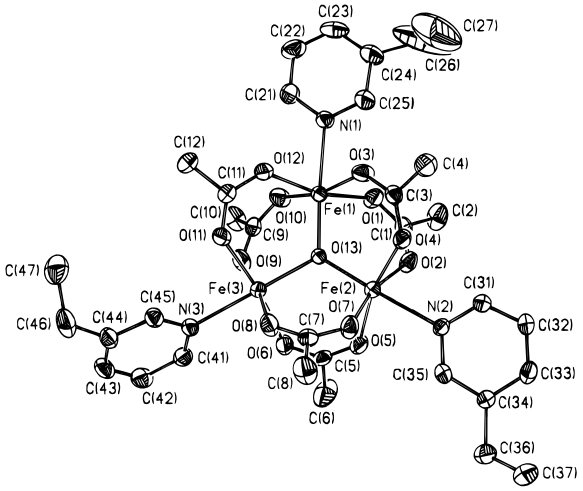

Figure 1. ORTEP plot of the molecular structure of the μ_3-oxo-bridged trinuclear complex in $[Fe_3O(O_2CCH_3)_6(3\text{-Et-py})_3]\cdot 0.5C_7H_8$ (**1**) at 298 K. Atoms are shown as 50% equiprobability ellipsoids.

Table 4. Selected Bond Distances and Angles for the Central Atoms of $[Fe_3O(O_2CCH_3)_6(3\text{-Et-py})_3]\cdot 0.5$(toluene) (**1**) at 297 K

Bond Distances (Å)			
Fe(1)−O(13)	1.858(4)	Fe(2)−N(2)	2.249(5)
Fe(2)−O(13)	1.866(4)	Fe(3)−N(3)	2.251(5)
Fe(3)−O(13)	2.006(4)	C(1)−O(1)	1.255(7)
Fe(1)−O(1)	2.067(4)	C(1)−C(2)	1.503(10)
Fe(1)−O(3)	2.044(4)	C(21)−N(1)	1.324(8)
Fe(2)−O(2)	2.053(4)	C(21)−C(22)	1.369(10)
Fe(2)−O(4)	2.054(4)	C(22)−C(23)	1.378(12)
Fe(3)−O(6)	2.090(5)	C(23)−C(24)	1.377(11)
Fe(3)−O(8)	2.125(5)	C(24)−C(26)	1.721(18)
Fe(1)−N(1)	2.252(5)	C(26)−C(27)	1.176(23)

Bond Angles (deg)			
Fe(1)−O(13)−Fe(2)	122.7(2)	O(3)−Fe(1)−O(13)	95.4(2)
Fe(1)−O(13)−Fe(3)	118.6(2)	O(1)−Fe(1)−O(10)	88.7(2)
Fe(2)−O(13)−Fe(3)	118.6(2)	O(3)−Fe(1)−O(12)	89.1(2)
N(1)−Fe(2)−O(13)	175.9(2)	O(3)−Fe(1)−O(12)	165.0(2)
N(2)−Fe(3)−O(13)	176.9(2)	O(3)−Fe(1)−O(10)	165.0(2)
N(3)−Fe(3)−O(13)	178.2(2)	N(1)−Fe(1)−O(1)	82.0(2)
O(1)−Fe(1)−O(13)	95.6(2)	N(1)−Fe(1)−O(3)	81.3(2)

Complex **1** crystallizes in the orthorhombic space group *Fdd*2 with $Z = 16$. Complex **1** is the first structurally characterized mixed-valence Fe_3O complex that does not belong to a rhombohedral or monoclinic space group. A perspective view of the molecular structure of **1** is depicted in Figure 1, and selected bond distances and angles are listed in Table 4. The planes of two of the three 3-Et-py ligands are nearly parallel to the Fe_3O plane, while the plane of the third ligand is closer to being perpendicular to the Fe_3O plane; dihedral angles between 3-Et-py ligand planes and the Fe_3O plane are 3.9, 5.4, and 66.3°.

In all of the X-ray structures reported for mixed-valence Fe_3O complexes, the pyridine ligands are very nearly parallel to or perpendicular to the Fe_3O plane.[6b,e,g,h,k] All four possible isomers having 3, 2, 1, or 0 pyridine ligands in the Fe_3O plane

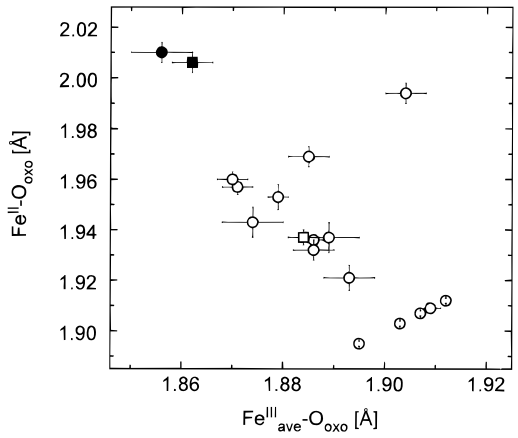

Figure 2. Correlation of Fe^{II}−O(oxide) and Fe^{III}−O(oxide) bond lengths from the reported[6,13] crystal structures of mixed-valence $[Fe_3O(O_2CR)_6(L)_3]\cdot S$ complexes. Data are shown for (■) $[Fe_3O(O_2CCH_3)_6(3\text{-Et-py})_3]\cdot 0.5C_6H_5CH_3$ (**1**) and (□) $[Fe_3O(O_2CCH_3)_6(4\text{-Et-py})_3]\cdot CH_3CCl_3$ (**4**), both at 298 K, and for (●) $[Fe_3O(O_2CCH_3)_6(4\text{-Et-py})_3]\cdot$4-Et-py at 163 K. The other data (○) are for complexes described in the literature.[6,13]

have been reported. It also has been found[6h] that the two asymmetric isomers with either 2 or 1 pyridine ligands in the Fe_3O plane exhibit ^{57}Fe Mössbauer spectra characteristic of relatively valence-trapped species. Clearly the conformation of the pyridine ligands is a major factor determining whether a complex can valence-detrap. When the three pyridine ligands are not symmetrically disposed, the three different vibronic states are not at the same energy. This will tend to trap a complex in one vibronic state. In the case of $[Fe_3O(O_2CCH_3)_6(4\text{-Et-py})_3]\cdot$4-Et-py,[6b] the planes of the two 4-Et-py ligands coordinated to the two Fe^{III} ions are perpendicular to the Fe_3O plane, while the plane of the 4-Et-py ligand bonded to the Fe^{II} ion is parallel. As the temperature of this 4-Et-py complex is increased, there is clear evidence in the Mössbauer spectrum of increasing rate of interconversion between the different vibronic states. It appears that the unique 4-Et-py ligand bonded to the Fe^{II} ion converts from a static disorder between two positions to a dynamic disorder. Thus, the onset of rotation of the unique 4-Et-py ligand affects the relative energies of the vibronic states and leads to an increase in the rate of interconversion. However, at the highest temperature (298 K) at which this 4-Et-py complex was studied, there are still two doublets in the Mössbauer spectrum.

An analysis of the bond lengths in complex **1** (Table 4) shows that this complex is the most valence-trapped complex reported at room temperature. In previous work[6h] we have shown that, for a series of mixed-valence Fe_3O complexes, there is a strong correlation between the Fe−O(oxide) and Fe−O(acetate) distances. This indicates that these distances reflect the oxidation state (average if the complex is dynamic) of the iron ion in a particular crystallographic site. For complex **1**, it is clear that the Fe(3) atom is unique and is the Fe^{II} ion: Fe(3)−O(oxide) = 2.006(4) Å; Fe(2)−O(oxide) = 1.866(4) Å; and Fe(1)−O(oxide) = 1.858(4) Å. Figure 2 shows a correlation of Fe^{II}−O(oxide) and Fe^{III}−O(oxide) bond lengths from the crystal structures of mixed-valence $[Fe_3O(O_2CR)_6(L)_3]\cdot S$ complexes.[6beghkno,13] Since there are two Fe^{III}−O(oxide) bond lengths in each complex, the Fe^{III}−O(oxide) value plotted in Figure 2 is an average value. There is a qualitative correlation of Fe^{II}−O(oxide) with Fe^{III}−O(oxide). The data for complex **1** at 298 K (■) clearly indicate that this complex is showing the most valence trapped structure at room temperature. The iron−oxide bond lengths of complex **1** at 298 K are very close to those [Fe^{II}−O = 2.010(4) Å and Fe^{III}−O(av) = 1.856(6) Å] of the valence-trapped structure of $[Fe_3O(O_2CCH_3)_6(4\text{-Et-py})_3]\cdot$4-Et-py at 163 K (●).[6b] The X-ray structure of the 4-Et-py complex at 298 K gives Fe^{II}−O = 1.953(5) Å and Fe^{III}−O(av) = 1.879(2) Å. There is much more dynamical averaging for the 4-Et-py complex at 298 K than for complex **1** at 298 K. Complex **1** is totally valence trapped at room temperature.

In Figure 3 is given a stereoview of the packing arrangement in complex **1**. It is interesting to try to identify what factors lead to valence trapping in complex **1**. There are only van der Waals interactions in the crystal of $[Fe_3O(O_2CCH_3)_6(3\text{-Et-py})_3]\cdot 0.5$(toluene) (**1**). There are no py···py overlaps characterizing the intermolecular interactions as in the stacked *R*32-symmetry Fe_3O complexes. Thus, even though complex **1** has only weak intermolecular interactions, it is totally valence trapped. In contrast, the stacked Fe_3O complexes with strong intermolecular interactions become valence detrapped at the higher temperatures. As can be seen in Figure 3, two Fe_3O molecules in complex **1** share one toluene solvate molecule that is located in the cavity made of six acetate ligands. The phenyl ring of the solvate toluene is almost perpendicular to the Fe_3O planes of the two neighboring Fe_3O complexes. Two 3-Et-py ligands, one from each of the two next-nearest Fe_3O complexes, also contact each toluene solvate. Thus, the toluene solvate molecule is wedged into a cavity of six acetate and two 3-Et-py ligands from neighboring complexes. Further examination of the packing in complex **1** shows that the three 3-Et-py ligands on each Fe_3 complex are also held relatively rigidly. In short, complex **1** is valence trapped because the planes of the three 3-Et-py ligands are not parallel and there is little motion permitted for the 3-Et-py ligands and the toluene solvate molecule.

In Figure 4 is shown a perspective drawing of the structure of the Fe_3O complex in $[Fe_3O(O_2CCH_3)_6(3\text{-Et-py})_3]\cdot CH_3CCl_3$ (**4**) determined at 238 K. Selected bond distances and angles are given in Table 5. Complex **4** crystallizes in the space group $P\bar{1}$ with two molecules in the unit cell. All three 3-Et-py ligands are coordinated to the iron ions with their molecular planes nearly perpendicular to the Fe_3O plane. The Fe_3O complex in **4** is distorted from an equilateral triangle at 238 K. The Fe−O(oxide) distances range from 1.874(3) to 1.937(3) Å. This 0.063 Å range is much smaller than the 0.148 Å range observed for complex **1**. The CH_3CCl_3 solvate molecule in the crystal of **4** is disordered between two positions such that one of the three Cl atoms and the $-CH_3$ group exchange their positions in an approximate ratio of 85/15, whereas the other two Cl atoms remain fixed in their positions.

In the crystal of complex **4**, the Fe_3O molecular units are arranged two-dimensionally in a layer where the CH_3CCl_3 solvate molecules are located in cavities made of three Fe_3O complexes. A stereo drawing of the packing arrangement of **4** is shown in Figure 5. This layer type of lattice structure and the orientations of 3-Et-py ligands relative to the Fe_3O plane closely resemble those of the above-mentioned layer type $[Fe_3O(O_2CCH_3)_6(3\text{-Me-py})_3]\cdot S$ complexes.

The room-temperature powder X-ray diffraction pattern for $[Fe_3O(O_2CCH_3)_6(3\text{-Et-py})_3]\cdot 0.5$ (benzene) (**2**) is very similar to that for $[Fe_3O(O_2CCH_3)_6(3\text{-Et-py})_3]\cdot 0.5$(toluene) (**1**) (see Figure 6). Also, the powder X-ray diffraction patterns for $[Fe_3O(O_2CCH_3)_6(3\text{-Et-py})_3]\cdot CH_3CN$ (**3**) and $[Fe_3O(O_2CCH_3)_6(3\text{-Et-}$

(13) (a) Ponomarev, V. I.; Filipenko, O. S.; Atovmyan, L. O.; Bobkova, S. A.; Turte, K. I. *Sov. Phys.−Dokl. (Engl. Transl.)* **1982**, *27*, 6. (b) Ponomarev, V. I.; Turte, K. I.; Shilov, G. V.; Bobkova, S. A.; Atovmyan, L. O.; Stukan, R. A. *Sov. J. Coord. Chem. (Engl. Transl.)* **1986**, *12*, 241. (c) Sato, T.; Nakamoto, T.; Katada, M.; Endo, K.; Sano, H. *Hyperfine Interact.* **1994**, *84*, 559.

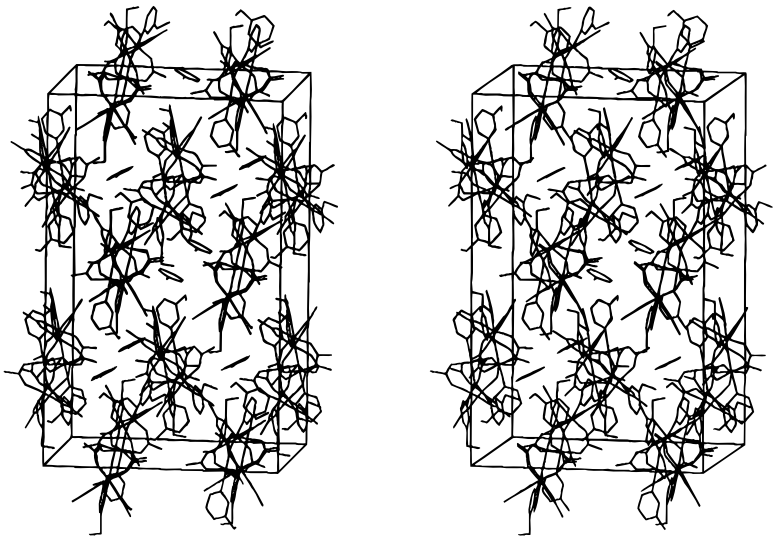

Figure 3. Stereoscopic view of the packing arrangement in $[Fe_3O(O_2CCH_3)_6(3\text{-Et-py})_3]\cdot 0.5(\text{toluene})$ (**1**).

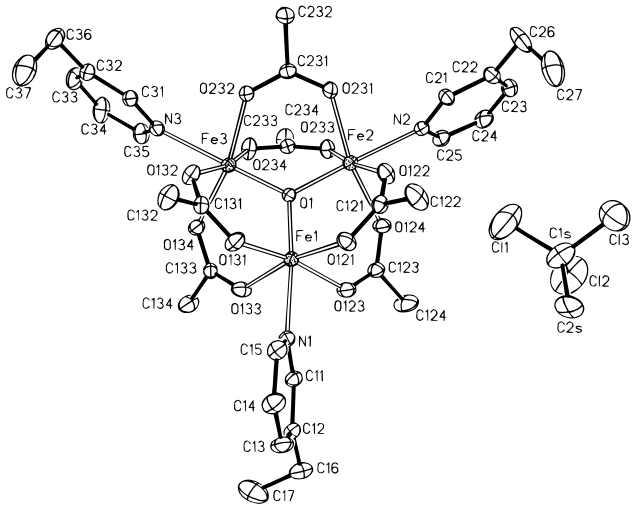

Figure 4. ORTEP plot of the molecular structure of the μ_3-oxo-bridged trinuclear complex in $[Fe_3O(O_2CCH_3)_6(3\text{-Et-py})_3]\cdot CH_3CCl_3$ (**4**) at 238 K. Atoms are shown as 50% equiprobability ellipsoids.

Table 5. Selected Bond Distances and Angles for the Central Atoms of $[Fe_3O(O_2CCH_3)_6(3\text{-Et-py})_3]\cdot CH_3CCl_3$ (**4**) at 238 K

Bond Distances (Å)			
Fe(1)−O(1)	1.894(2)	Fe(2)−N(2)	2.227(4)
Fe(2)−O(1)	1.937(3)	Fe(3)−N(3)	2.239(4)
Fe(3)−O(1)	1.874(3)	C(131)−O(131)	1.243(6)
Fe(1)−O(121)	2.056(4)	C(131)−C(132)	1.511(5)
Fe(1)−O(123)	2.061(3)	C(11)−N(1)	1.345(50
Fe(2)−O(122)	2.071(3)	C(11)−C(12)	1.380(5)
Fe(2)−O(124)	2.074(3)	C(12)−C(13)	1.379(5)
Fe(3)−O(132)	2.056(2)	C(13)−C(14)	1.384(7)
Fe(3)−O(134)	2.056(3)	C(12)−C(16)	1.512(6)
Fe(1)−N(1)	2.230(3)	C(16)−C(17)	1.493(10)
Bond Angles (deg)			
Fe(1)−O(1)−Fe(2)	119.2(2)	O(123)−Fe(1)−O(1)	98.0(1)
Fe(1)−O(1)−Fe(3)	121.1(1)	O(121)−Fe(1)−O(131)	86.8(1)
Fe(2)−O(1)−Fe(3)	119.7(1)	O(123)−Fe(1)−O(133)	87.6(1)
N(1)−Fe(1)−O(1)	175.2(1)	O(121)−Fe(1)−O(133)	169.0(1)
N(2)−Fe(2)−O(1)	177.3(1)	O(123)−Fe(1)−O(131)	167.0(1)
N(3)−Fe(3)−O(1)	178.8(1)	N(1)−Fe(1)−O(121)	86.6(1)
O(121)−Fe(1)−O(1)	97.4(1)	N(1)−Fe(1)−O(123)	84.6(1)

$py)_3]\cdot CH_3CCl_3$ (**4**) are very similar (see Figure 6). From these XRD patterns, it can be concluded that the half-solvate complexes **1** and **2** are isostructural (space group *Fdd*2) but are structurally different from complexes **3** and **4**, which have a full solvate molecule (space group $P\bar{1}$) and a layer type of lattice.

^{57}Fe Mössbauer Spectroscopy. Variable-temperature Mössbauer spectra were collected for the four complexes $[Fe_3O(O_2CCH_3)_6(3\text{-Et-py})_3]\cdot S$, where S is 0.5(toluene) (**1**), 0.5(benzene) (**2**), CH_3CN (**3**), and CH_3CCl_3 (**4**). It was found that the hemisolvate complexes **1** and **2** are valence trapped from 120 to 298 K on the Mössbauer time scale. Complexes **3** and **4** are shown to be valence trapped below ~100 K, whereas increasing the temperature leads to valence detrapping near room temperature.

In Figure 7 are given some Mössbauer spectra for the toluene solvate complex **1** taken in the range 57−350 K. At all temperatures least-squares fitting of the spectra to Lorentzian line shapes clearly indicates that each spectrum is composed of only two quadrupole-split doublets. Table 6 summarizes the Mössbauer fitting parameters for complex **1**. In each spectrum the more intense doublet corresponds to the two high-spin Fe^{III} ions and the less intense doublet is for the one high-spin Fe^{II} ion. The ratio of Fe^{III} to Fe^{II} signals is 1.87 at 57 K and increases gradually to 2.68 at 350 K. It is not unreasonable to expect a high-spin Fe^{III} ion to experience a recoilless fraction that is somewhat larger than that of a high-spin Fe^{II} ion in the same crystal at 350 K. The center shift for each of the two doublets (uncorrected for second-order Doppler shift) is plotted versus temperature in Figure 8. At all temperatures complex **1** remains valence trapped. This is made clear by the comparison shown in Figure 8 where center shift data reported for the Fe^{II} ion in $[Cr^{III}_2Fe^{II}O(O_2CCH_3)_6(py)_3]\cdot$ py and for the Fe^{III} ion in $[Fe^{III}_2Co^{II}O(O_2CCH_3)_6(py)_3]\cdot$py are plotted versus temperature.[6b] The temperature dependencies of the center shifts observed for the Fe^{II} and Fe^{III} ions in complex **1** are very close to those for the iron ions in $[Cr^{III}_2Fe^{II}O(O_2CCH_3)_6(py)_3]\cdot$py and $[Fe^{III}_2Co^{II}O(O_2CCH_3)_6(py)_3]\cdot$py. Complex **1** is fully valence trapped even at 350 K. In the case of the isostructural benzene solvate complex **2**, ^{57}Fe Mössbauer spectra show characteristics and fitting parameters very similar to those found for complex **1** (see Figure 9A and Table 7). Thus, complex **2** is also valence trapped from 120 to 298 K on the Mössbauer time scale.

In contrast to the behavior of the hemisolvated complexes **1** and **2**, the other solvated complexes **3** and **4** show a temperature-dependent Mössbauer behavior. As shown in Figure 9B, the CH_3CN solvate complex **3** is partially valence detrapped at 298 K on the Mössbauer time scale (see Table 7 for fitting parameters). In the case of the CH_3CCl_3 solvate complex **4**, it is also clear that this complex exhibits valence detrapping on

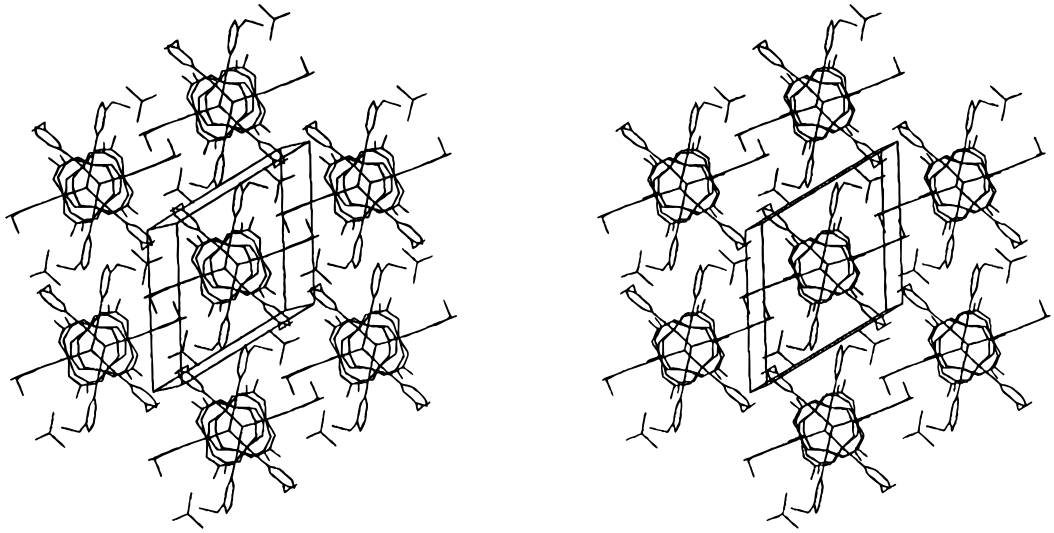

Figure 5. Stereoscopic view of the packing arrangement in $[Fe_3O(O_2CCH_3)_6(3\text{-Et-py})_3]\cdot CH_3CCl_3$ (**4**).

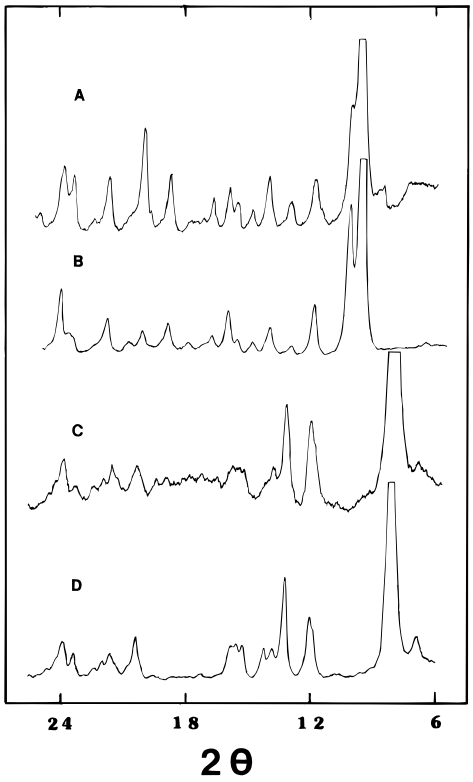

Figure 6. Room-temperature powder X-ray diffraction patterns: (A) $[Fe_3O(O_2CCH_3)_6(3\text{-Et-py})_3]\cdot 0.5$(toluene) (**1**); (B) $[Fe_3O(O_2CCH_3)_6(3\text{-Et-py})_3]\cdot 0.5$(benzene) (**2**); (C) $[Fe_3O(O_2CCH_3)_6(3\text{-Et-py})_3]\cdot CH_3CN$ (**3**); (D) $[Fe_3O(O_2CCH_3)_6(3\text{-Et-py})_3]\cdot CH_3CCl_3$ (**4**).

the Mössbauer time scale when the sample temperature is increased (see Figure 10). At 43 K, the spectrum of complex **4** consists of two doublets; one is characteristic of high-spin Fe^{II} and the other is characteristic of high-spin Fe^{III} with an area ratio of 2:1. All fitting parameters obtained for complex **4** are given in Table 8. At room temperature (293 K), complex **4** shows a single doublet that is an average signal for all three Fe ions in the Fe_3O complex.

From the results on the variable-temperature Mössbauer spectra and the X-ray structures of these four $[Fe_3O(O_2CCH_3)_6(3\text{-Et-py})_3]\cdot S$ complexes, it is evident that the lattice packing environments of these Fe_3O complexes can control whether a given complex can become valence detrapped. The isostructural complexes **1** and **2** are valence trapped up to room temperature,

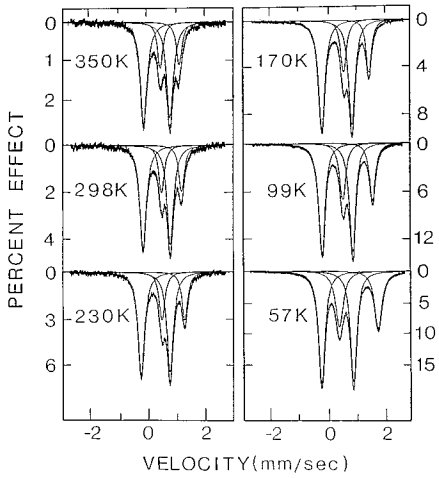

Figure 7. Variable-temperature ^{57}Fe Mössbauer spectra for $[Fe_3O(O_2CCH_3)_6(3\text{-Et-py})_3]\cdot 0.5$(toluene) (**1**).

whereas the isostructural complexes **3** and **4** are completely valence detrapped near room temperature.

The valence detrapping and indirectly the intramolecular electron rate are less sensitive to the size and shape of the solvate molecule in these layer type structures found in complexes **3** and **4** than what was found for the stack type structure (space group *R*32) in $[Fe_3O(O_2CCH_3)_6(4\text{-Me-py})_3]\cdot S$.[6k] From the data on the $[Fe_3O(O_2CCH_3)_6(4\text{-Me-py})_3]\cdot S$ series, it was found that small variations in the sizes and shapes of the solvate molecules (*e.g.*, S = $CHCl_3$, CH_3CCl_3, or CH_3CHCl_3) lead to considerable changes (~30−45 deg) in the temperatures for valence detrapping. Despite the relatively large differences in size and shape between the CH_3CN solvate molecule in complex **3** and the CH_3CCl_3 solvate molecule in complex **4**, these two complexes become valence-detrapped at about the same temperature (~300 K). The different levels of sensitivity of valence detrapping temperature to the solvate molecule could be attributed to the different magnitudes of intermolecular interactions in these two types of lattice structures, layer versus stack types. In the stacked Fe_3O complexes there are strong intermolecular interactions as the result of the overlap of pyridine ligands between neighboring complexes. In the case of these stacked complexes, each solvate molecule is located in the cavity between two Fe_3O complexes in one stack. These solvate molecules are involved only in van der Waals interactions with the Fe_3O complexes. However, the nature (size and shape) of the solvate molecule

Table 6. ^{57}Fe Mössbauer Fitting Parameters[a] for $[Fe_3O(O_2CCH_3)_6(3\text{-Et-py})_3]\cdot 0.5(\text{toluene})$ (**1**)

	δ, mm/s[b]		ΔE_Q, mm/s		Γ, mm/s[c]		% area	
T, K	Fe^{III}	Fe^{II}	Fe^{III}	Fe^{II}	Fe^{III}	Fe^{II}	Fe^{III}	Fe^{II}
57	0.532(0)	1.254(0)	1.052(0)	1.176(1)	0.129(0)	0.138(1)	65.2(2)	34.8(2)
					0.131(0)	0.137(1)		
99	0.531(0)	1.242(1)	1.039(1)	1.051(1)	0.126(1)	0.125(1)	66.2(2)	33.8(0)
					0.130(1)	0.123(1)		
170	0.530(1)	1.181(1)	0.995(1)	0.878(1)	0.129(1)	0.114(1)	70.0(2)	30.0(2)
					0.132(1)	0.113(1)		
230	0.531(1)	1.121(1)	0.959(1)	0.776(1)	0.128(2)	0.114(1)	70.4(2)	29.6(2)
					0.132(2)	0.114(1)		
298	0.532(2)	1.032(1)	0.905(1)	0.678(3)	0.127(1)	0.111(2)	71.4(2)	28.6(2)
					0.131(1)	0.113(3)		
350	0.537(2)	0.976(2)	0.873(2)	0.640(3)	0.131(2)	0.105(3)	72.8(2)	27.2(2)
					0.140(3)	0.113(3)		

[a] Peaks were least-squares-fit to Lorentzian line shapes with equal areas for both components of a doublet; error in the last significant figure is given in the parentheses. [b] Center shifts relative to iron metal at room temperature. [c] Half-width at half-maximum listed in order of increasing velocity of the peak.

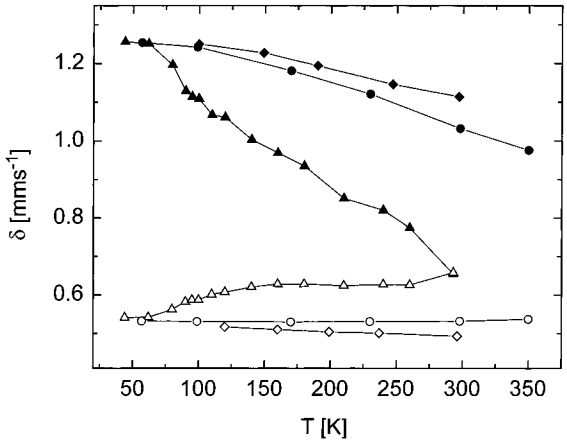

Figure 8. Plot of the center shift (δ) relative to α-iron versus temperature for the "Fe^{II}" (closed symbols) and "Fe^{III}" (open symbols) doublets in the spectra of $[Fe_3O(O_2CCH_3)_6(3\text{-Et-py})_3]\cdot 0.5(\text{toluene})$ (**1**) (○ and ●), $[Fe_3O(O_2CCH_3)_6(3\text{-Et-py})_3]\cdot CH_3CCl_3$ (**4**) (△ and ▲), $[Cr^{III}_2Fe^{II}O(O_2CCH_3)_6(py)_3]\cdot py$ (◆), and $[Fe^{III}_2Co^{II}O(O_2CCH_3)_6(py)_3]\cdot py$ (◇). Lines connecting data points for one complex are drawn to guide the eye only.

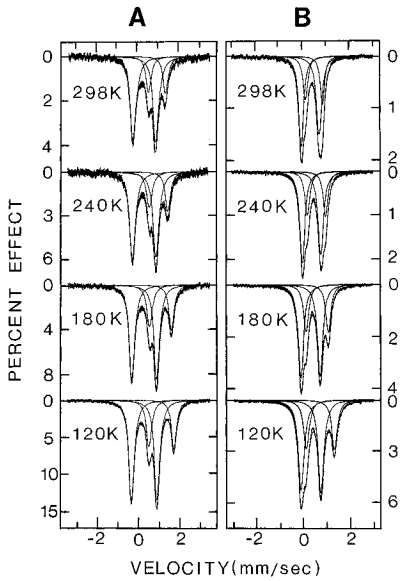

Figure 9. Variable-temperature ^{57}Fe Mössbauer spectra for (A) $[Fe_3O(O_2CCH_3)_6(3\text{-Et-py})_3]\cdot 0.5(\text{benzene})$ (**2**) and (B) $[Fe_3O(O_2CCH_3)_6(3\text{-Et-py})_3]\cdot CH_3CN$ (**3**).

probably affects the strong py···py intermolecular interactions. In contrast, in the layer Fe_3O complexes there are no very strong intermolecular interactions between neighboring Fe_3O complexes.

Finally, the Mössbauer spectra for the CH_3CCl_3 solvate **4** were examined carefully in order to understand in more detail the valence-detrapping process. When the Mössbauer spectra for **4** were fitted, it was necessary to fit each spectrum with two asymmetric doublets (Fe^{III} and Fe^{II} sites) where each doublet has two Lorentzian features of equal area but of different line widths. In Figure 11 the line widths of these four components of the two doublets are plotted as a function of temperature. It can be seen that the line widths of the four lines are close to each other at temperatures up to 62 K, but in the region of ∼70 to ∼160 K the line width of the high-velocity component of the "Fe^{II}" doublet increases to a significantly larger value than the other three components. In other words, the line widths of the two "Fe^{III}" components and the low-velocity "Fe^{II}" component remain relatively constant (line width $\Gamma = 0.15 \pm 0.03$ mm/s), whereas Γ for the high-velocity "Fe^{II}" component exhibits a surge from 0.15 to 0.27 mm/s, back to 0.12 mm/s. From Figure 8 it can be seen that it is also in the 60−70 K range where the center shifts of the Fe^{III} and Fe^{II} ions in complex **4** begin to show some effects of averaging. In short, the two doublets move together to become a single average doublet without any significant changes in line widths except in the high-velocity "Fe^{II}" component.

Valence-Detrapping Process. What is occurring in the solid state when the Fe_3O complexes in **3** and **4** convert from valence trapped at low temperatures to valence detrapped at higher temperatures? By reference to Figure 12,[6f,14] which shows two possible potential-energy surfaces for the ground state of an $Fe^{III}_2Fe^{II}O$ complex, it is possible to understand the valence-detrapping process. The potential-energy surface can have either three or four minima depending on the ratio (Δ) of the electronic coupling and the vibronic coupling. At low temperatures (<∼50 K) all parts of the crystal lattices of these complexes are static. Because of the low symmetry for the crystal site of a Fe_3O complex, one minimum of the three or four minima on the potential-energy surface is at lower energy than the other minima. The Fe_3O complex is valence trapped with the complex distorted so that there is one Fe^{II} ion and two Fe^{III} ions. When the temperature of the crystal is increased above ∼50 K, there are basically two things that could occur. Either the potential-energy surface remains relatively unchanged as the temperature is increased or as a result of changes in the crystal and/or Fe_3O complex the potential-energy surface changes.

(14) Nakano, M.; Sorai, M.; Vincent, J. B.; Christou, G.; Jang, H. G.; Hendrickson, D. N. *Inorg. Chem.* **1989**, *28*, 4608.

Table 7. ^{57}Fe Mössbauer Fitting Parameters[a] for $[Fe_3O(O_2CCH_3)_6(3\text{-Et-py})_3]\cdot S$ Complexes

	δ, mm/s[b]		ΔE_Q, mm/s		Γ, mm/s[c]		% area	
T, K	Fe^{III}	Fe^{II}	Fe^{III}	Fe^{II}	Fe^{III}	Fe^{II}	Fe^{III}	Fe^{II}
			A. $[Fe_3O(O_2CCH_3)_6(3\text{-Et-py})_3]\cdot 05(benzene)_{0.5}$					
120	0.528(1)	1.241(1)	1.072(1)	1.055(2)	0.135(1)	0.133(2)	68.6(2)	31.4(2)
					0.137(1)	0.127(2)		
180	0.524(1)	1.185(2)	1.043(2)	0.919(3)	0.138(2)	0.138(2)	69.0(2)	31.0(2)
					0.140(2)	0.130(3)		
240	0.521(2)	1.053(3)	1.024(3)	0.786(6)	0.145(2)	0.142(6)	70.6(2)	29.4(2)
					0.149(2)	0.130(7)		
298	0.520(2)	0.957(2)	1.016(3)	0.717(6)	0.150(3)	0.130(4)	71.6(2)	28.4(2)
					0.146(3)	0.126(4)		
			B. $[Fe_3O(O_2CCH_3)_6(3\text{-Et-py})_3]\cdot CH_3CN$					
120	0.624(1)	1.084(2)	0.992(2)	1.286(4)	0.173(2)	0.166(4)	66.0(2)	34.0(2)
					0.137(1)	0.127(2)		
180	0.652(1)	0.992(2)	0.956(2)	1.110(3)	0.156(2)	0.151(3)	67.0(2)	33.0(2)
					0.140(2)	0.130(3)		
240	0.650(1)	0.915(1)	0.919(2)	0.912(2)	0.145(2)	0.145(3)	68.6(2)	31.4(2)
					0.156(2)	0.139(3)		

[a] Peaks were least-squares-fit to Lorentzian line shapes with equal areas for both components of a doublet; errors in the last significant figure are given in the parentheses. [b] Center shifts relative to iron metal at room temperature. [c] Half-width at half-maximum listed in order of increasing velocity of the peak.

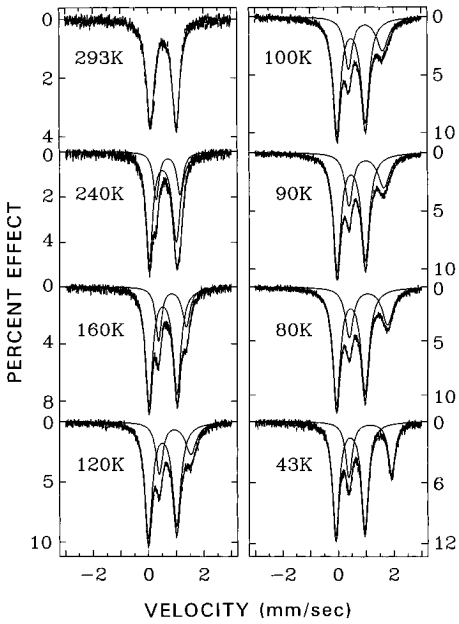

Figure 10. Variable-temperature ^{57}Fe Mössbauer spectra for $[Fe_3O(O_2CCH_3)_6(3\text{-Et-py})_3]\cdot CH_3CCl_3$ (**4**).

In the case of a relatively temperature-independent potential-energy surface, what types of processes can occur? There is a barrier for conversion from the lowest-energy minimum (*i.e.*, where the "extra" electron resides on one iron ion, the Fe^{II} ion) to the other minima. An increase in temperature gives greater thermal energy, and at some temperature the Fe_3O complex can convert from the lowest-energy minimum to the others (this corresponds to an electron transfer for the extra electron from one iron ion to another). This process could occur by a classical thermal activation over a barrier, or the Fe_3O complex could be thermally activated to a higher-energy vibrational level and then tunnel from one minimum to another. In either case, the expectation is that as the temperature is increased, the rate of interconversion between minima would increase. The above Mössbauer data and other data[5,6] (*e.g.*, heat capacity and ^{2}H NMR data for other mixed-valence Fe_3O complexes) do not agree with this. Thus, if the rate of interconversion between minima were increasing with increasing temperature, the two doublets seen at low temperature for complex **4** should coalesce. Each component of the Fe^{III} doublet averages with one component of the Fe^{II} doublet. The ^{57}Fe Mössbauer technique is sensitive to processes with rates in the range of $\sim 10^6 - 10^9$ s^{-1}. If the rate of interconversion of a Fe_3O complex is less than this at low temperatures and becomes greater than 10^9 s^{-1} at higher temperatures, there should be line-broadening effects seen for all of the components of the two doublets in the temperature range where the rate goes through the Mössbauer window. This is not what is seen for complex **4** or for other mixed-valence Fe_3O complexes[6] and mixed-valence biferrocene complexes.[7]

The other possibility is that the potential-energy surface changes as the temperature is increased. However, there is always a barrier for interconversion. The mixed-valence Fe_3O complexes never become electronically delocalized, where as a result of an increase in electronic coupling there are no barriers for interconversion. The presence of barriers has been established through an analysis of variable-temperature IR data.[6p] This analysis shows that on the vibrational time scale ($\sim 10^{-15}$ s) there are distinct Fe^{III} and Fe^{II} ions.

It is possible to explain the observed Mössbauer data for the present and previously studied Fe_3O complexes by the following model. At low temperatures (<50 K) one minimum on the surface is at much lower energy than the others and the Fe_3O complex is valence trapped. When the temperature is increased, the solvate molecules convert from static to dynamic. Substituted pyridine ligands also may become somewhat dynamic. The net result is that each Fe_3O complex feels a symmetrized environment. The relatively large-amplitude motions of the solvate molecules and ligands give an effective C_3-symmetry Fe_3O complex. Now at least three minima on the potential-energy ground-state surface are at the same energy. In this case it seems reasonable to expect that a given Fe_3O complex could quantum mechanically tunnel between the three equal-energy vibronic states at a rate in excess of 10^9 s^{-1}. In this case, the ^{57}Fe Mössbauer technique would "see" an average-valence Fe_3O complex. One average doublet would be seen. This dynamic environment with rapidly tunneling Fe_3O complexes is what is meant by valence detrapped.

The important phenomenon that remains to be explained is the absence of line broadening observed in the Mössbauer spectra in the intermediate-temperature region. This is done by presuming there are domains in the crystals where either valence-trapped or valence-detrapped complexes are present in the intermediate-temperature region. When a Fe_3O complex is

Table 8. ^{57}Fe Mössbauer Fitting Parameters[a] for $[Fe_3O(O_2CCH_3)_6(3\text{-Et-py})_3]\cdot CH_3CCl_3$ (**4**)

	δ, mm/s[b]			ΔE_Q, mm/s			Γ, mm/s[c]			% area		
T, K	Fe^{III}	Fe^{Av}	Fe^{I}	Fe^{III}	Fe^{Av}	Fe^{II}	Fe^{III}	Fe^{Av}	Fe^{II}	Fe^{III}	Fe^{Avg}	Fe^{II}
43	0.541(1)		1.256(3)	1.041(3)		1.537(5)	0.145(2)		0.144(5)	67.0(7)		33.0(7)
							0.151(2)		0.149(5)			
62	0.542(1)		1.251(2)	1.032(2)		1.485(5)	0.158(2)		0.158(5)	68.0(6)		32.0(6)
							0.164(2)		0.162(5)			
80	0.562(1)		1.196(3)	1.024(2)		1.372(5)	0.162(2)		0.176(5)	68.1(6)		31.9(6)
							0.179(2)		0.234(7)			
90	0.582(1)		1.129(3)	1.018(2)		1.254(6)	0.162(2)		0.168(5)	68.4(8)		31.6(8)
							0.179(2)		0.256(8)			
95	0.587(1)		1.114(4)	1.022(3)		1.223(8)	0.163(3)		0.163(7)	68.9(10)		31.1(10)
							0.182(3)		0.241(10)			
100	0.587(1)		1.109(4)	1.021(2)		1.222(7)	0.159(2)		0.174(6)	67.2(9)		32.8(9)
							0.176(3)		0.268(10)			
110	0.601(1)		1.067(3)	1.019(2)		1.143(6)	0.168(2)		0.165(5)	69.4(9)		30.6(9)
							0.186(2)		0.241(8)			
120	0.607(1)		1.060(5)	1.019(3)		1.138(9)	0.161(3)		0.152(7)	70.2(12)		29.8(12)
							0.180(3)		0.243(11)			
140	0.620(2)		1.003(5)	1.012(3)		1.048(8)	0.151(3)		0.137(7)	70.8(14)		29.2(14)
							0.169(3)		0.199(10)			
160	0.628(2)		0.969(4)	1.010(3)		1.001(3)	0.152(3)		0.126(7)	72.5(14)		27.5(14)
							0.170(3)		0.171(9)			
180	0.628(2)		0.935(5)	1.001(3)		0.954(7)	0.145(3)		0.124(7)	72.0(16)		28.0(16)
							0.165(4)		0.160(8)			
210	0.624(3)		0.851(5)	0.981(4)		0.891(7)	0.139(4)		0.129(8)	69.4(23)		30.6(23)
							0.167(4)		0.148(8)			
240	0.627(5)		0.820(8)	0.976(6)		0.864(11)	0.145(6)		0.123(12)	73.1(36)		26.9(36)
							0.177(6)		0.135(11)			
260	0.626(6)		0.774(7)	0.961(6)		0.865(9)	0.142(7)		0.124(12)	69.6(50)		30.4(50)
							0.178(6)		0.118(9)			
293		0.654(2)			0.927(4)			0.166(3)			100.0	

[a] Peaks were least-squares-fit to Lorentzian line shapes with equal areas for both components of a doublet; error in the last significant figure is given in the parentheses. [b] Center shifts relative to iron metal at room temperature. [c] Half-width at half-maximum listed in order of increasing velocity of the peak.

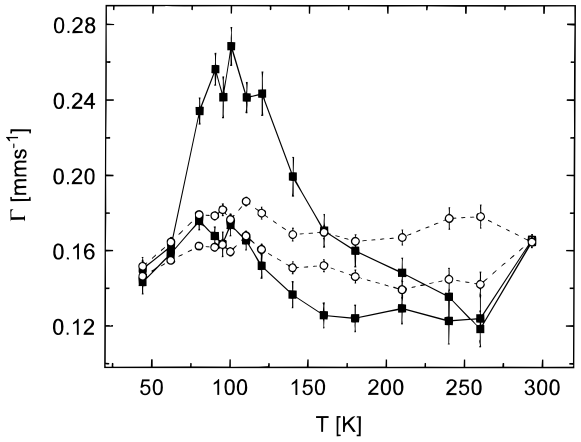

Figure 11. Plot of line widths (half-width at half-maximum) versus temperature for the "Fe^{III}" (○) and "Fe^{II}" (■) doublets in the spectra of $[Fe_3O(O_2CCH_3)_6(3\text{-Et-py})_3]\cdot CH_3CCl_3$ (**4**). Straight lines are drawn to connect data points for the "Fe^{II}" doublets.

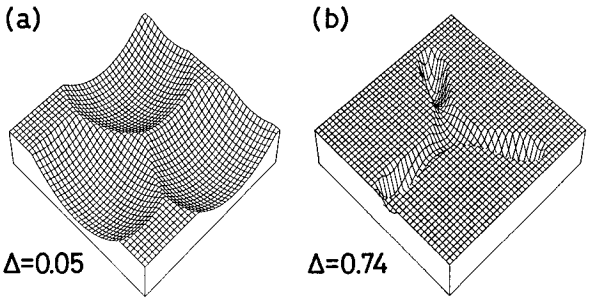

Figure 12. Adiabatic potential energy surface[14] for the ground state of a mixed-valence M_3O complex calculated for two different values of $(\Delta/kw)/\lambda^2$, where w is the electron-transfer integral between two metal ions, λ gauges the strength of the vibronic interaction, and the force constant for the molecular distortion is k: (a) $\Delta = 0.5$; (b) $\Delta = 0.74$.

in a domain where the environment is relatively static, it is valence trapped. When it is in a domain where the environment is dynamic, it is tunneling at a rate fast compared to the Mössbauer time scale. Domain walls are the regions between the two types of domains. If the domain walls are moving about the crystal at a rate faster than the Mössbauer technique can sense, this could lead to the absence of line width broadening due to a coalescence phenomenon. At a particular temperature in the intermediate region, a certain fraction of complexes are in "static" domains, while the other complexes are in the "dynamic" domains. The net result is that the Fe^{II} doublet picks up some character of the Fe^{III} doublet and *vice versa*. An increase in temperature changes the ratio of Fe_3O complexes in static *versus* dynamic domains. The two Mössbauer doublets move together and eventually when all complexes are in dynamic domains, only a single average doublet is seen. Thus, the temperature dependence seen in Figure 10 for complex **4** is not a reflection of complexes experiencing faster and faster rates of electron transfer. Instantaneously there are only trapped or detrapped complexes relative to the Mössbauer time scale. Only the effects of increasing lattice dynamics are being seen, and the rate of the lattice dynamics exceeds the Mössbauer time scale.

The above explanation works particularly well to rationalize the complete absence of line-broadening effects for variable-temperature Mössbauer spectra of mixed-valence biferrocene complexes. In the case of complex **4**, the high-velocity component of the "Fe^{II}" doublet does show a surge in line width in the ~70−160 K region (Figure 11). Such asymmetry of quadrupole doublets in Mössbauer spectra observed for some iron complexes has been interpreted as a result of the fluctuating electric and magnetic fields produced by the relaxation of

paramagnetic species containing the ^{57}Fe nucleus.[15] However this oscillating-field relaxation model fails to account for the details of the line broadening in complex **4**. First an asymmetry of quadrupole doublets should be observed for *both* "Fe^{III} and Fe^{II}" ions in an oscillating-field model. Second, as the relaxation rate of the fluctuating electric and magnetic fields becomes comparable to the Zeeman frequencies [precession frequencies corresponding to the different transitions between the excited (ex) and ground (gr) nuclear states], instead of the high-velocity component ($|\pm^1/_2>_{gr} \leftrightarrow |\pm^1/_2>_{ex}$), the low-velocity component ($|\pm^1/_2>_{gr} \leftrightarrow |\pm^3/_2>_{ex}$) of the "$Fe^{II}$" doublet should exhibit a greater line width due to its higher Zeeman frequencies in such a fluctuating field. Finally, the absence of the magnetic hyperfine patterns for the complex **4** at low temperatures cannot be explained with a fluctuating field generated by the relaxation of a paramagnetic ion or a group of magnetically coupled paramagnetic ions, whereas a magnetic pattern is expected to occur when the frequencies of the fluctuating field slow down as the temperature is decreased.

In agreement with the observation of line broadening and the order−disorder transition of a solvate molecule in an Fe^{II} spin-crossover complex[16] and the results of the past studies on solvate dynamics in several Fe_3O systems,[6c,e,g,h,k,l] the line-broadening behavior in complex **4** probably reflects the onset of the motion associated with the CH_2CCl_3 solvate molecule. If the CH_3CCl_3 solvate molecules are experiencing increasing rates and amplitudes of motion in the temperature region, then the Fe^{II} Mössbauer signal, in particular the high-velocity component, would be most responsive to this. The Fe^{II} ion has a larger quadrupole splitting than does the Fe^{III} ion and would be more responsive to the onset of dynamics associated with parts of the crystal.

Acknowledgment. This work was supported by NSF Grant CHE-9420322 (D.N.H.) and NIH Grant HL-13652 (D.N.H.). D.N.H. thanks the Humboldt Foundation for a Humboldt-Forschungspreis in 1993.

Supporting Information Available: Tables of bond lengths, bond angles, anisotropic displacement coefficients, and hydrogen coordinates and isotropic displacement coefficients for the X-ray structures of $[Fe_3O(O_2CCH_3)_6(3\text{-Et-py})_3 \cdot 0.5C_6H_5CH_3$ (**1**) at 298 K and $[Fe_3O(O_2CCH_3)_6(3\text{-Et-py})_3] \cdot CH_3CCl_3$ (**4**) at 238 K (10 pages). Ordering information is given on any current masthead page.

IC9514509

(15) (a) Wickman, H. H.; Trozzolo, A. M. *Phys. Rev. Lett.* **1965**, *15*, 156. (b) Blume, M. *Phys. Rev. Lett.* **1965**, *14*, 96.

(16) König, E.; Ritter, G.; Kulshreshtha, S. K.; Waigel, J.; Sacconi, L. *Inorg. Chem.* **1984**, *23*, 1241.